2-19-2019

Maternal inflammation at midgestation impairs subsequent fetal myoblast function and skeletal muscle growth in rats, resulting in intrauterine growth restriction at term

Caitlin N. Cadaret
University of Nebraska - Lincoln

Robert J. Posont
University of Nebraska - Lincoln

Kristin A. Beede
University of Nebraska Lincoln, kristin.beede@unl.edu

Hannah E. Riley
University of Nebraska - Lincoln

John Dustin Loy
University of Nebraska-Lincoln, jdloy@unl.edu

See next page for additional authors

Maternal inflammation at midgestation impairs subsequent fetal myoblast function and skeletal muscle growth in rats, resulting in intrauterine growth restriction at term[1]

Caitlin N. Cadaret,* Robert J. Posont,* Kristin A. Beede,* Hannah E. Riley,* John Dustin Loy,† and Dustin T. Yates*,[2]

*Department of Animal Science, University of Nebraska–Lincoln, Lincoln, NE 68583; and †School of Veterinary Medicine and Biomedical Sciences, University of Nebraska–Lincoln, Lincoln, NE 68583

ABSTRACT: Maternal inflammation induces intrauterine growth restriction (MI-IUGR) of the fetus, which compromises metabolic health in human offspring and reduces value in livestock. The objective of this study was to determine the effect of maternal inflammation at midgestation on fetal skeletal muscle growth and myoblast profiles at term. Pregnant Sprague-Dawley rats were injected daily with bacterial endotoxin (MI-IUGR) or saline (controls) from the 9th to the 11th day of gestational age (dGA; term = 21 dGA). At necropsy on dGA 20, average fetal mass and upper hindlimb cross-sectional areas were reduced ($P < 0.05$) in MI-IUGR fetuses compared with controls. MyoD$^+$ and myf5$^+$ myoblasts were less abundant ($P < 0.05$), and myogenin$^+$ myoblasts were more abundant ($P < 0.05$) in MI-IUGR hindlimb skeletal muscle compared with controls, indicating precocious myoblast differentiation. Type I and Type II hindlimb muscle fibers were smaller ($P < 0.05$) in MI-IUGR fetuses than in controls, but fiber type proportions did not differ between experimental groups. Fetal blood plasma TNFα concentrations were below detectable amounts in both experimental groups, but skeletal muscle gene expression for the cytokine receptors *TNFR1*, *IL6R*, and *FN14* was greater ($P < 0.05$) in MI-IUGR fetuses than controls, perhaps indicating enhanced sensitivity to these cytokines. Maternal blood glucose concentrations at term did not differ between experimental groups, but MI-IUGR fetal blood contained less ($P < 0.05$) glucose, cholesterol, and triglycerides. Fetal-to-maternal blood glucose ratios were also reduced ($P < 0.05$), which is indicative of placental insufficiency. Indicators of protein catabolism, including blood plasma urea nitrogen and creatine kinase, were greater ($P < 0.05$) in MI-IUGR fetuses than in controls. From these findings, we conclude that maternal inflammation at midgestation causes muscle-centric fetal programming that impairs myoblast function, increases protein catabolism, and reduces skeletal muscle growth near term. Fetal muscle sensitivity to inflammatory cytokines appeared to be enhanced after maternal inflammation, which may represent a mechanistic target for improving these outcomes in MI-IUGR fetuses.

Key words: adaptive fetal programming, developmental origins, inflammatory regulation, maternofetal stress, thrifty phenotype

[1]This manuscript is based on research that was partially supported by the National Institute of General Medical Sciences Grant 1P20GM104320 (J. Zempleni, Director), the Nebraska Agricultural Experiment Station with funding from the Hatch Act (Accession Number 1009410) and Hatch Multistate Research capacity funding program (Accession Numbers 1011055, 1009410) through the USDA National Institute of Food and Agriculture. The Biomedical and Obesity Research Core (BORC) in the Nebraska Center for Prevention of Obesity Diseases (NPOD) receives partial support from NIH (NIGMS) COBRE IDeA award NIH 1P20GM104320. The contents of this publication are the sole responsibility of the authors and do not necessarily represent the official views of the NIH or NIGMS. The authors have no conflicts of interest to declare.

[2]Corresponding author: dustin.yates@unl.edu

Received February 4, 2019.

Accepted March 29, 2019.

Transl. Anim. Sci. 2019.3:867–876
doi: 10.1093/tas/txz037

INTRODUCTION

Maternal stress during gestation induces intrauterine growth restriction (IUGR), which is linked to lifelong deficits in skeletal muscle growth and metabolic dysfunction in humans and livestock (Yates et al., 2016, 2018). Late prenatal and postnatal muscle growth requires proliferation, differentiation, and fusion of myoblasts with existing muscle fibers (Zhu et al., 2004), and this rate-limiting process can be altered by inflammation (Langen et al., 2001, 2004; Posont et al., 2018). Inflammatory changes within the skeletal muscle niche can arise from systemic inflammation and from resident macrophages within the tissue itself (Kharraz et al., 2013). Acute inflammation impairs adult myoblast function in vitro (Frost et al., 1997; Langen et al., 2001), and we hypothesized that maternal inflammation may likewise disrupt fetal myoblast function and muscle growth in utero. The programming effects of fetal stress on muscle development and growth have implications for long-term metabolic health in IUGR-born humans and growth performance in livestock (Zhu et al., 2004; Yates et al., 2011, 2012), but the underlying mechanisms are not well understood. Our previous studies in placental insufficiency-induced IUGR fetal sheep have identified intrinsically impaired myoblast function and restricted muscle growth as outcomes of unidentified molecular adaptations (Yates et al., 2012, 2014, 2016). Therefore, the objective of this study was to determine the effects of sustained maternal inflammation at midgestation on myoblast profiles, muscle growth, and metabolic indicators at term.

MATERIALS AND METHODS

Animals and Experimental Design

Animal procedures were approved by the Institutional Animal Care and Use Committee at the University of Nebraska–Lincoln. Animal studies were performed at the University of Nebraska–Lincoln Animal Science Complex, which is accredited by AAALAC International. Timed-pregnant Sprague-Dawley rats (Envigo, Indianapolis, IN) were purchased and delivered on the 6th day of gestational age (dGA). Beginning at dGA 8, rats were individually housed, fed commercial rat chow ad libitum, and weighed daily. From the 9th to the 11th dGA, rats were randomly assigned to be injected (i.p.) daily with 250-µL physiological saline (control, $n = 9$) or 0.1 µg/kg BW of lipopolysaccharide (LPS) endotoxin from *E. coli* O55:B5 (Sigma–Aldrich, St. Louis, MO) in 250-µL physiological saline to create maternal inflammation-induced IUGR (MI-IUGR, $n = 10$). Maternal blood samples were collected via saphenous vein puncture and rectal temperatures were recorded at 3, 6, and 24 h after each of the daily injections. On dGA 20 (term = 21 dGA), rats were euthanized by decapitation under heavy isoflurane anesthesia and maternal blood samples were collected. Litter size and individual fetal weights were recorded, and skinned hindlimbs were collected from the 3 fetuses in each litter located closest to the uterine bifurcation. The right hindlimb from each fetus was snap frozen, and the left hindlimb was fixed in 4% paraformaldehyde. Pooled blood samples were collected from the remaining fetuses in each litter via exsanguination.

Blood Analysis

Glucose concentrations were determined from maternal and fetal whole blood in duplicate with a Contour next EZ glucose meter (Bayer Corp., Whippany, NJ). Blood plasma was then isolated by centrifugation (14,000 × *g*, 2 min, 4 °C), and TNFα concentrations were determined in duplicate by Rat TNFα Quantikine ELISA kit (R&D Systems, Minneapolis, MN) as previously described (Seo et al., 2017). Interassay and intra-assay coefficient of variation was less than 10%, and the detection limit was 5 pg/mL. Fetal blood plasma concentrations of urea nitrogen (BUN), high-density lipoprotein cholesterol (HDLC), total cholesterol, triglycerides, and total protein were determined via colorimetric assays with a Vitros-250 Chemistry Analyzer (Ortho Clinical Diagnostics, Linden, NJ) according to manufacturer recommendations. Concentrations of γ-glutamyltransferase (GGT), aspartate aminotransferase (AST), and alanine aminotransferase (ALT) were determined via multiple-point rate assays with the Vitros-250 Chemistry Analyzer.

Gene Expression

RNA isolation. RNA was extracted from frozen fetal hindlimb muscle (~30 mg) via RNeasy Fibrous Tissue Mini Kit (Qiagen, Germantown, MD). For all samples, isolated RNA was quantified on a NanoDrop microvolume spectrophotometer (Thermo Fisher, Waltham, MA) and reverse transcribed into cDNA via QuantiTect Reverse Transcription Kit (Qiagen).

Droplet Digital PCR. Primer pairs for PCR were designed for the genes of interest listed in Table 1. Droplet Digital PCR (ddPCR) was performed in duplicate with the QX200 ddPCR System (Bio-Rad, Hercules, CA). Each reaction contained Evagreen Supermix, 10 µM of each primer, and equivalent amounts of cDNA template. Droplets were generated in a QX200 Droplet Generator with Droplet Generator Oil, transferred to a PCR plate, sealed, and placed in a C1000 Touch Thermal Cycler. Samples were activated (95 °C for 5 min), denatured for 40 cycles (95 °C for 30 s), annealed and extended for 40 cycles (60 °C for 1 min), and stabilized (4 °C for 5 min and 90 °C for 5 min). Finally, droplets were read on the QX200 Droplet Reader, and results were analyzed with QuantaSoft Software (Bio-Rad) to obtain transcripts per microliter for genes of interest. Results were normalized to transcripts per microliter of *YWHAZ*, which was stable across treatment groups.

Immunohistochemistry

Myoblast profiles. Fixed fetal hindlimbs were embedded in OCT Compound (Thermo Fisher). Tissue cross-sections cut at a thickness of 8 µm were taken at the midpoint of the femur, prepared with a CryoStar NX50 (Thermo Fisher), and mounted on glass microscope slides as previously described (Yates et al., 2014). Slides were dried at 37 °C for 30 min and then washed 3 times in phosphate-buffered saline (PBS) + 0.5% Triton-X-100. Antigen retrieval was performed by boiling slides in 10 mM citric acid for 20 min and allowing them to cool slowly to room temperature. Nonspecific binding was blocked by incubating slides with 0.5% NEN blocking buffer (Perkin-Elmer, Waltham, MA) in PBS at room temperature for 1 h. Slides were then incubated overnight at 4 °C with primary antibodies diluted in PBS + 1% bovine serum albumin (Sigma–Aldrich). Negative controls were incubated in PBS + 1% bovine serum albumin without primary antibody. Sections were stained with antibodies raised in the rabbit against myf5 (1:100; Santa Cruz, Dallas, TX), in the mouse against myoD (1:200; Dako, Santa Clara, CA), and in the mouse against myogenin (1:250, Abcam, Cambridge, MA) to identify nuclei expressing these myogenic factors. Immunocomplexes were detected with affinity-purified immunoglobulin antiserum conjugated to Alexa Fluor 594 (1:2,000; Cell Signaling, Danvers, MA) or Alexa Fluor 488 (1:1,000; Cell Signaling). Myoblast profiles were assessed in the medial and lateral muscle groups, which included the adductor and gracilis muscles and the semitendinosus, semimembranosus, and biceps femoris, respectively.

Muscle fiber profiles. A second set of hindlimb cross-sections were stained to identify fiber type ratios and fiber size as previously described (Yates et al., 2016). Briefly, fibers in medial and lateral muscle groups expressing myosin heavy chain (MyHC) isoforms specific for Type I and Type II fibers were identified with antibodies raised in the mouse against MyHC-I (BA-D5, 1:20; Developmental Studies Hybridoma Bank (DSHB),

Table 1. Primers for Droplet Digital PCR

Gene	Protein	Primer sequence	Product size	Accession number
ADRB1	β1 Adrenoceptor	GGGAGTACGGCTCCTTCTTC	45	NM_012701
		CGTCTACCGAAGTCCAGAGC		
ADRB2	β2 Adrenoceptor	AGCCACCTACGGTCTCTGAA	208	NM_012492.2
		GTCCCGTTCCTGAGTGATGT		
ADRB3	β3 Adrenoceptor	TTGCCTCCAATATGCCCTAC	46	NM_013108
		AAGGAGACGGAGGAGGAGAG		
FN14	TWEAK receptor	CACTGATCCAGTGAGGAGCA	88	NM_181086
		GGCAATTAGACACCCTGGAA		
IL6R	IL-6 receptor	CACGAGCCATCATGAAGAGA	96	NM_017020
		GCCAAGGTGCTTGGATTTTA		
TNFR1	TNFα receptor 1	TTGTAGGATTCAGCTCCTGTC	109	NM_013091
		CTCTTACAGGTGGCACGAAGTT		
YWHAZ	14-3-3 protein ζ	CCGAGCTGTCTAACGAGGAG	88	NM_013011
		GAGACGACCCTCCAAGATGA		

University of Iowa, Iowa City, IA) and MyHC-II (F18, 1:25; DSHB), respectively. Muscle sections were counterstained with antibodies raised in the rabbit against desmin (1:1,000, Sigma–Aldrich) to identify all fibers. Immunocomplexes were detected with affinity-purified immunoglobulin antiserum conjugated to Alexa Fluor 594 (1:2,000) or Alexa Fluor 488 (1:1,000). All fluorescent images were visualized on an Olympus IX73 and digital micrographs were captured with a DP80 microscope camera (Olympus, Center Valley, PA). Images were analyzed with Olympus cellsSens Dimension software to determine proportions of positive nuclei or fibers within fetal skeletal muscle sections. Animal identifications and treatments were deidentified prior to analyses.

Statistical Analysis

All data were analyzed by analysis of variance using the mixed procedure of SAS 9.4 (SAS Institute, Cary, NC) to determine the effect of experimental group. Repeated measures were used for serial maternal measurements. Skeletal muscle gene expression data are expressed as transcript copies per microliter, normalized to copies per microliter of *YWHAZ*. Proportions of nuclei staining positive for myogenic regulatory factors were determined from a minimum of 250 positive nuclei, counted across 6 nonoverlapping fields of view per fetus. Skeletal muscle fiber type proportions were determined from a minimum of 2,500 total fibers counted across 3 fields of view per fetus. Average fiber size was determined from a minimum of 250 fibers across 3 fields of view per fetus. Rat (dam) was considered the experimental unit for all variables, and values were averaged across the fetuses analyzed in each dam's litter. All data are expressed as group mean ± SE.

RESULTS

Maternal Responses to Lipopolysaccharide Administration

Experimental group × time point interactions were observed ($P < 0.05$) for maternal rectal temperatures and plasma TNFα concentrations, but not for maternal plasma glucose concentrations. Maternal rectal temperatures in MI-IUGR dams were greater ($P < 0.05$) than in control dams at 6, 30, 54, and 72 h after beginning the daily injections on dGA 9 (Fig. 1A), but were not different from control temperatures at the other measured time points. Maternal blood glucose did not differ between experimental groups (Fig. 1B). Maternal plasma TNFα concentrations in control dams were below the detectable limit (5 pg/mL) at all time points except for 24 h, when 5 of the 9 controls exhibited plasma TNFα concentrations between 5 and 16.5 pg/mL. Plasma TNFα concentrations were increased ($P < 0.05$) in MI-IUGR dams at 3, 6, 24, 27, and 51 h after beginning daily injections (Fig. 1C). Maternal weights and daily feed intake did not differ between the 2 experimental groups on any day.

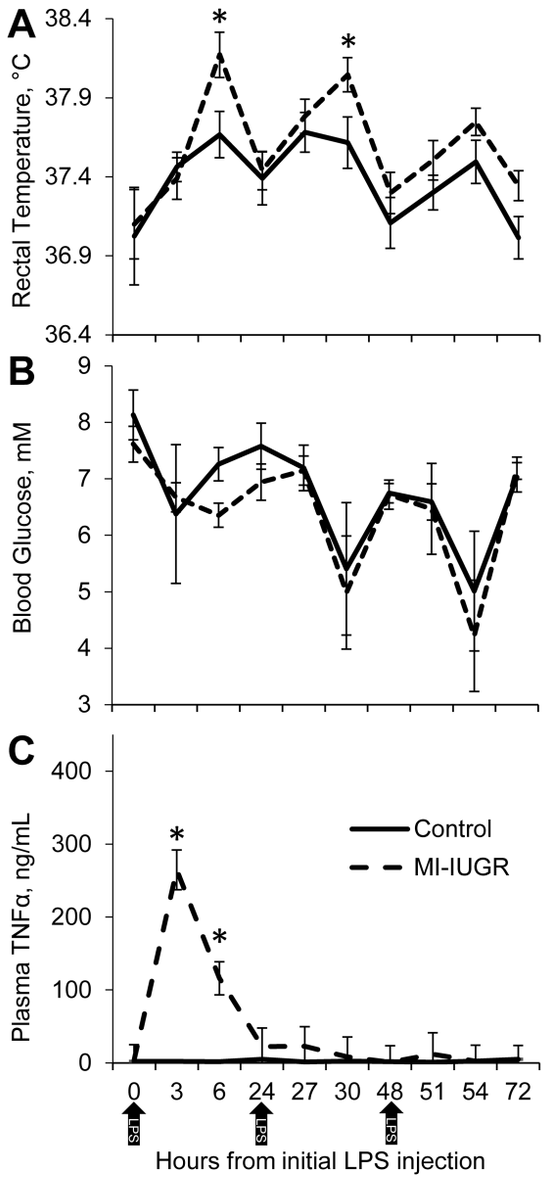

Figure 1. Maternal responses to daily lipopolysaccharide (LPS) endotoxin injection (0.1 µg/kg BW; i.p.). Pregnant rats were injected with LPS (MI-IUGR; $n = 10$) or saline (control; $n = 9$) from the 9th to the 11th day of gestation (shown by arrows). Rectal temperatures (A) were measured by digital thermometer. Glucose concentrations (B) were measured in whole blood via glucose meter, and TNFα concentrations (C) were measured in blood plasma via ELISA. *Means differed ($P < 0.05$) between experimental groups for the time period.

Fetal Morphometrics and Blood Chemistry

At necropsy, the number of fetuses per litter did not differ between controls and MI-IUGR (14.2 ± 0.6 and 13.1 ± 0.6, respectively), but average fetal mass and upper hindlimb area were reduced ($P < 0.05$) in MI-IUGR fetuses compared with controls (Fig. 2). Plasma TNFα concentrations at necropsy were below detectable limits (5 pg/mL) in all fetuses and in all dams with the exception of 2 MI-IUGR dams that exhibited 8 and 24 pg/mL, respectively. Maternal blood glucose concentrations did not differ between experimental groups at necropsy, but fetal blood glucose was decreased ($P < 0.05$) in MI-IUGR fetuses compared with controls (Table 2). Fetal BUN concentrations were increased ($P < 0.05$) in MI-IUGR fetuses compared with controls. Plasma HDLC concentrations did not differ between control and MI-IUGR fetuses. Plasma cholesterol and triglyceride concentrations were reduced ($P < 0.05$) in MI-IUGR fetuses compared with controls. Plasma total protein content did not differ between control and MI-IUGR fetuses. Plasma AST, ALT, and creatine kinase were greater ($P < 0.05$) in MI-IUGR fetuses compared with controls. Fetal plasma GGT did not differ between experimental groups.

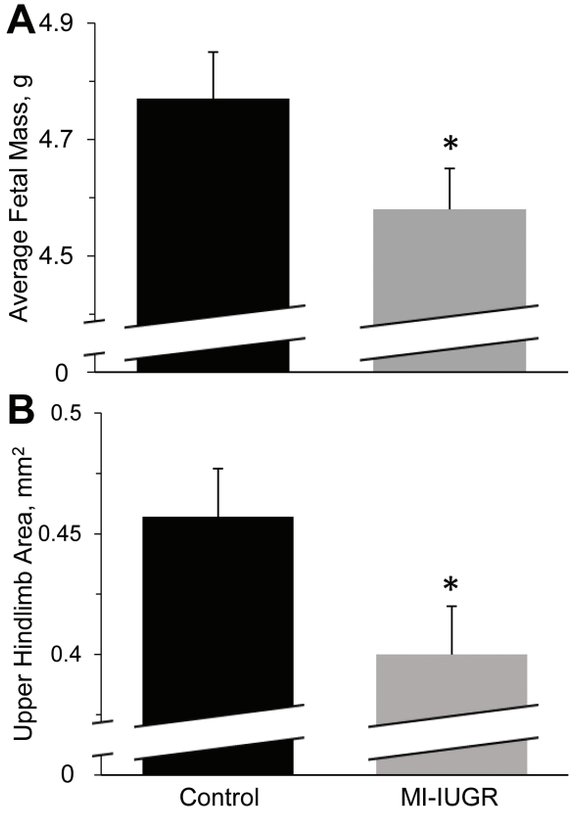

Figure 2. Average fetal mass (A) and upper hindlimb area (B) for MI-IUGR ($n = 10$) and control ($n = 9$) fetal rats on the 20th day of gestation. Average fetal mass was determined by weighing all fetuses in each litter. Upper hindlimb cross-sectional area at the midpoint of the femur was averaged for the 3 fetuses in each litter located closest to the uterine bifurcation. *Means differed ($P < 0.05$) between experimental groups.

Skeletal Muscle Gene Expression

Skeletal muscle *TNFR1* (TNFα receptor 1), *FN14* (TWEAK receptor), and *IL6R* (IL-6 receptor) expression were increased ($P < 0.05$) in MI-IUGR fetuses compared with controls (Table 3). Skeletal muscle *ADRB1* (β1 adrenoceptor) mRNA was lower ($P < 0.05$) in MI-IUGR fetuses compared with controls, but skeletal muscle *ADRB2* (β2 adrenoceptor) and *ADRB3* (β3 adrenoceptor) mRNA content did not differ between experimental groups. Skeletal muscle mRNA expression for the pan macrophage marker *CD68* (cluster of differentiation 68) was decreased ($P < 0.05$) in MI-IUGR fetuses compared with controls. Fetal skeletal muscle mRNA expression for the M2-macrophage marker *CD163* (cluster of differentiation 163) did not differ between experimental groups.

Skeletal Muscle Myoblast Profiles

Representative micrographic images are shown for myoblast populations staining positive for myf5 (Fig. 3A), myoD (Fig. 3B), and myogenin (Fig. 3C) in fetal hindlimb skeletal muscle. At necropsy, MI-IUGR decreased ($P < 0.05$) the number of myf5$^+$ and myoD$^+$ nuclei (Fig. 3D and E, respectively) and increased ($P < 0.05$) the number of myogenin$^+$ nuclei (Fig. 3F) in fetal hindlimb muscle compared with controls.

Skeletal Muscle Fiber Type Proportions and Sizes

Representative micrographic images are shown for muscle fiber populations staining positive for MyHC-I (Type I; Fig. 4A) and MyHC-II (Type II; Fig. 4B) in fetal hindlimb skeletal muscle. At necropsy, the average cross-sectional area of Type I and Type II fibers in hindlimb skeletal muscle were smaller ($P < 0.05$) in MI-IUGR fetuses compared with controls (Fig. 4C and D, respectively). The proportions of Type I and Type II fibers in fetal hindlimb skeletal muscle did not differ between experimental groups.

DISCUSSION

In this study, we found that maternal inflammation at midgestation impaired subsequent fetal

Table 2. Blood components in maternal inflammation-induced intrauterine growth restriction (MI-IUGR) fetal rats

Parameter[1]	Control	MI-IUGR	*P*-value
Blood glucose, mM			
Maternal	6.7 ± 0.3	7.2 ± 0.3	NS[2]
Fetal	2.5 ± 0.2	2.0 ± 0.2	0.01
Maternal–fetal ratio	2.8 ± 0.3	3.6 ± 0.4	0.01
Fetal blood plasma			
BUN, mg/dL	20.0 ± 0.2	23.9 ± 0.8	<0.01
Cholesterol, mg/dL	51.0 ± 0.3	45.0 ± 0.2	<0.01
HDLC, mg/dL	20.1 ± 1.4	18. ± 1.1	NS
Triglycerides, mg/dL	71.3 ± 1.9	61.5 ± 1.5	<0.01
Total protein, g/dL	1.77 ± 0.09	1.71 ± 0.08	NS
AST, IU/L	124.8 ± 8.9	159.8 ± 13.5	0.02
ALT, IU/L	56.9 ± 1.4	66.2 ± 5.2	<0.01
Creatine kinase, IU/L	5355 ± 393	9045 ± 1001	<0.01
GGT, IU/L	15.9 ± 0.3	16.4 ± 1.0	NS

[1]BUN = blood plasma urea nitrogen; HDLC = high-density lipoprotein cholesterol; AST = aspartate transaminase; ALT = alanine transaminase; GGT = gamma-glutamyltransferase.

[2]NS = not significant.

Table 3. Gene expression[1] in skeletal muscle from maternal inflammation-induced intrauterine growth restriction (MI-IUGR) fetal rats

Gene[2]	Control	MI-IUGR	*P*-value
TNFR1	0.50 ± 0.05	0.86 ± 0.22	0.01
IL6R	0.42 ± 0.06	0.62 ± 0.09	<0.01
FN14	0.13 ± 0.01	0.21 ± 0.03	0.04
ADRB1	0.46 ± 0.09	0.30 ± 0.05	0.09
ADRB2	0.21 ± 0.02	0.21 ± 0.01	NS[3]
ADRB3	0.18 ± 0.04	0.24 ± 0.07	NS
CD68	0.23 ± 0.04	0.13 ± 0.02	0.03
CD163	0.16 ± 0.03	0.15 ± 0.04	NS

[1]Transcripts/*YWHAZ* transcripts.

[2]*TNFR1* = TNFα receptor 1; *IL6R* = IL-6 receptor; *FN14* = TWEAK receptor; *ADRB1* = β1 adrenoceptor; *ADRB2* = β2 adrenoceptor; *ADRB3* = β3 adrenoceptor; *CD68* = cluster of differentiation 68; *CD163* = cluster of differentiation 163.

[3]NS = not significant.

myoblast function, reduced fetal muscle growth, and led to an IUGR phenotype at term. Systemic inflammation was not apparent at term in these dams or their fetuses. However, the sensitivity of fetal skeletal muscle to inflammatory cytokines appeared to be enhanced due to greater gene expression for cytokine receptors. This coincided with indicators of reduced myoblast proliferation and precocious differentiation, diminished muscle fiber hypertrophy, and smaller hindlimb areas. Fetal programming by maternal inflammation also increased indicators of protein catabolism in fetal blood plasma at term. Fetal hypoglycemia and reduced fetal-to-maternal glycemic ratios were indicative of placental insufficiency, which would help to explain how maternal inflammation at midgestation resulted in the fetal changes observed near term. The evidence for enhanced cytokine sensitivity, impaired myoblast function, and increased protein catabolism in this study provide insight into a potential programming mechanism for the predisposition of IUGR-born offspring to poor muscle growth and metabolism.

The first of the 3 daily injection of LPS caused a temporal increase in maternal circulating TNFα and body temperatures that peaked at 3 to 6 h and was gone by 24 h. Interestingly, the maternal response to the subsequent injections was less profound, perhaps due to a reduced sensitivity of the immune system to the endotoxin. Furthermore, the impact of the endotoxin on maternal well-being beyond the period of administration appeared to be minimal, as daily intake, average daily gain, glycemic levels, and circulating TNFα concentrations subsequent to the final injection were comparable to controls. Conversely, maternal inflammation at midgestation caused changes in fetal skeletal muscle that remained present at term, well after the inflammation had subsided. Greater gene expression for cytokine receptors in MI-IUGR fetal muscle are evidence of enhanced sensitivity to inflammatory cytokines despite low circulating TNFα that suggests an absence of systemic fetal inflammation near term. Skeletal muscle is highly responsive to inflammatory cytokines (Frost et al., 1997; Cadaret et al., 2017), and increased inflammatory activity can disrupt muscle growth. Thus,

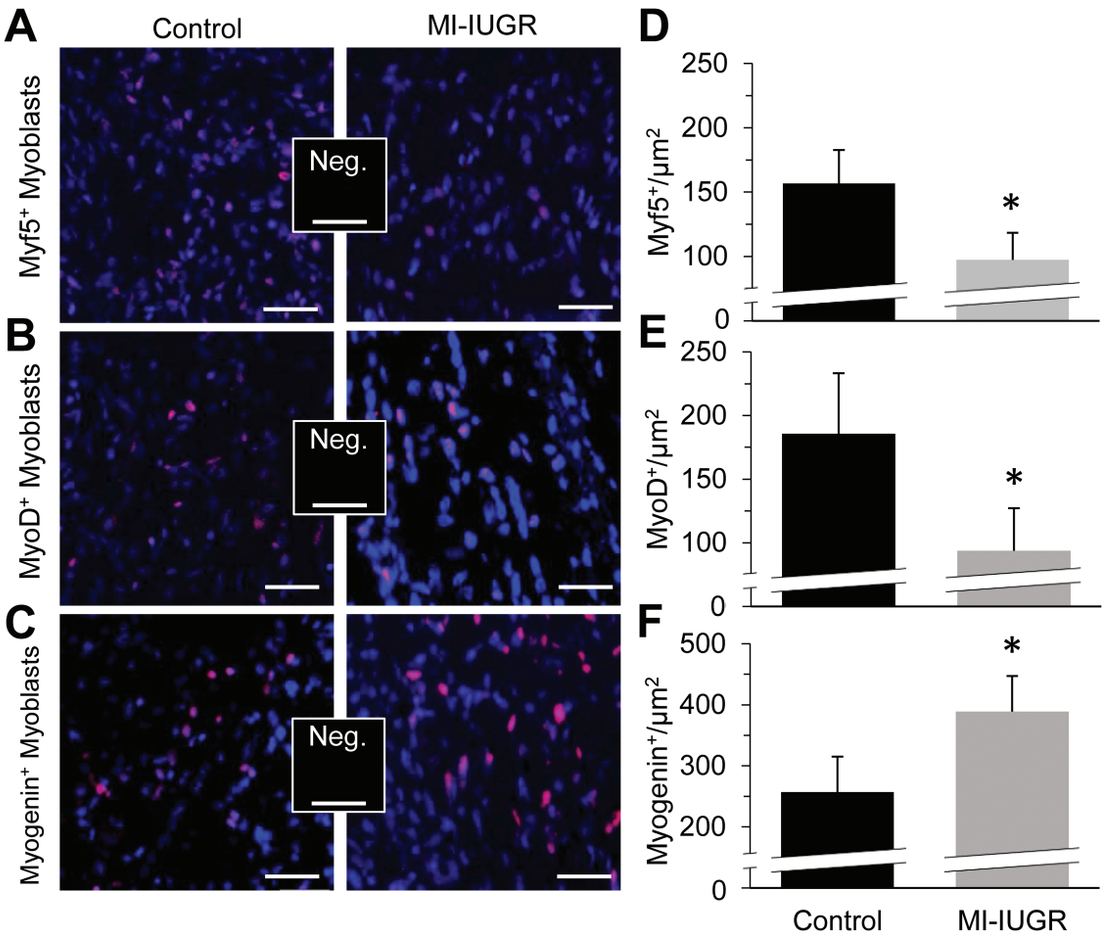

Figure 3. Myoblast profiles in MI-IUGR (n = 10) and control (n = 9) fetal rats on the 20th day of gestation. Representative micrographs are shown for fetal myoblasts staining positive for myf5 (A; red), myoD (B; red), and myogenin (C; red), and counterstained with DAPI (blue). The number of nuclei staining positive for myf5 (D), myoD (E), and myogenin (F) per µm^2 were determined from fixed cross-sections of the upper hindlimb of the 3 fetuses in each litter located closest to the uterine bifurcation. *Means differed (P < 0.05) between experimental groups.

it is possible that greater inflammatory tone caused by increased cytokine sensitivity contributed to reduced fetal muscle growth in this study, although a more in-depth evaluation of this potential mechanism is warranted.

Smaller fetal myofiber size following maternal inflammation was coincident with impaired fetal myoblast function, which is consistent with our previous findings in placental insufficiency-induced IUGR fetal sheep (Yates et al., 2014; Posont et al., 2018). At term, medial and lateral hindlimb muscles of MI-IUGR fetal rats had fewer nuclei expressing myoD and myf5, which are indicative of myoblasts in the proliferative stage (Kitzmann et al., 1998) prior to differentiating (Rudnicki et al., 1993). In addition, more nuclei stained positive for myogenin, which is expressed by myoblasts that have exited the cell cycle and begun differentiating (Rawls et al., 1995). These transcription factor profiles indicate precocious entry of fetal myoblasts into terminal differentiation at the expense of proliferation, which would conform with greater sensitivity to inflammatory cytokines. The effect of cytokines on myoblast function is complex, but increased activity of IL-6/IL6R pathways has been shown to increase myoblast differentiation and correlates with greater myogenin expression (Hoene et al., 2013). Although TNFα/TNFR1 and TWEAK/Fn14 pathways antagonize myoblast differentiation in many cases, their increased activity has also been shown to diminish myoD in myoblasts (Langen et al., 2004; Dogra et al., 2006), as observed in the present study. Paradoxical reductions in gene expression for macrophage indicators in this study may be indicative of a compensatory reduction in resident macrophages, particularly M1 macrophages, which are important contributors to the proliferation-inducing myoblast niche (Du et al., 2017). The lack of changes in β2 and β3 adrenoceptor gene expression following maternal inflammation was somewhat surprising, as both have anti-inflammatory properties (Lirussi et al., 2008; Kolmus et al., 2014). Previous studies have shown that less β1 adrenergic activity (indicated

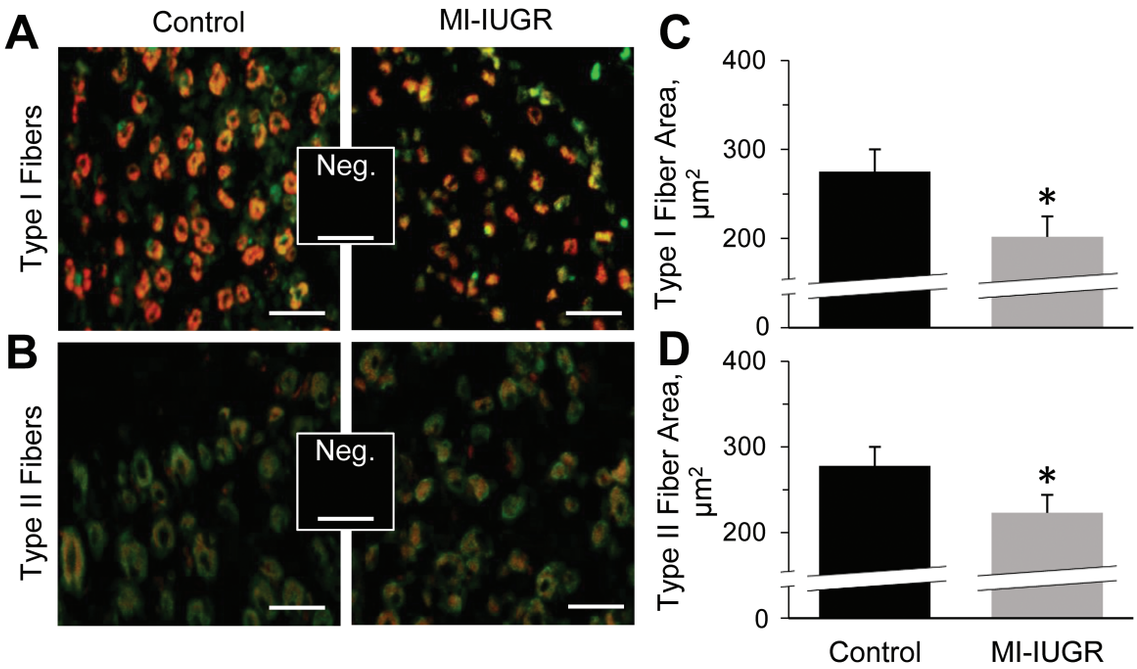

Figure 4. Skeletal muscle fiber sizes in MI-IUGR (n = 10) and control (n = 9) fetal rats on the 20th day of gestation. Representative micrographs are shown for fetal hindlimb muscle fibers staining positive for MyHC-1 (A; Type I fibers; red) and MyHC-2 (B; Type II fibers; red), and counterstained for desmin (green). The average cross-sectional areas of Type I (C) and Type II (E) muscle fibers were determined from fixed cross-sections of the upper hindlimb of the 3 fetuses in each litter located closest to the uterine bifurcation. *Means differed (P < 0.05) between experimental groups.

by reduced receptor gene expression is our study) could be associated with greater inflammation (Ardestani et al., 2017), but it would be unlikely that less β1 activity would affect myoblast function directly (Church et al., 2014).

Greater BUN concentrations indicate that protein catabolism was increased near term in MI-IUGR fetuses (Depner, 2001), perhaps to provide an energy substrate to compensate for hypoglycemia and reduced circulating triglycerides (Lemons and Schreiner, 1983). Indeed, a previous study in IUGR fetal sheep, which were hypoglycemic by ~50%, found that fetal urea production was ~2.5-fold greater than in controls (Jensen et al., 1999). In IUGR-born rats, BUN continued to be greater at 3 mo of age (He et al., 2015), indicating that it is a programmed change. Higher circulating creatine kinase, AST, and ALT concentrations in our MI-IUGR fetuses are further evidence of increased muscle protein catabolism (Depner, 2001; Nie et al., 2011; Bodie et al., 2016). Greater protein catabolic rates together with reductions in protein accretion observed in IUGR fetal sheep (Rozance et al., 2018) would presumably contribute to the reduction in hindlimb muscle fiber size in our MI-IUGR fetuses.

Mechanisms linking maternal inflammation and muscle-centric fetal programming were not directly evaluated in this study, but fetal hypoglycemia in the presence of maternal euglycemia would indicate that placental insufficiency was present. A previous study in rats showed that daily maternal LPS injections in the early third trimester reduced trophoblast invasion and spiral artery remodeling in the placenta (Cotechini et al., 2014b). These changes were accompanied by reductions in placental weight, area, and thickness (Cotechini et al., 2014a). Enhanced gene expression for cytokine receptors observed in our MI-IUGR fetuses could have also been the result of direct fetal inflammation, as chronic inflammatory events have been shown to increase *TNFR1* and *IL6R* in other tissues (Lam et al., 2008; Liu et al., 2016). Placental permeability to maternal inflammatory cytokines is low (Aaltonen et al., 2005), but the rodent placenta is at least somewhat permeable to LPS (Kohmura et al., 2000). Thus, it is possible that the fetus produced its own inflammatory response to LPS transferred from maternal to fetal circulation. However, other studies indicate that the placenta itself is a more likely source for fetal inflammation, as maternal LPS administration has been shown to increase placental cytokine production substantially (Bloise et al., 2013).

From these findings, we can conclude that muscle-centric fetal programming by maternal inflammation at midgestation impairs fetal myoblast function and increases fetal protein catabolism.

These changes were associated with impaired skeletal muscle growth, which contributed to IUGR at term. The role of these changes in postnatal muscle mass deficits of IUGR-born offspring was not clear from the present study but may be a reasonable aim for future studies with this model. Likewise, it was unclear if the muscle-centric fetal programming events observed in this study were survival adaptations by the fetus, but reduced skeletal muscle would allow reappropriation of limited fetal nutrients to neural and cardiac tissues. Thus, it is important for future studies seeking to moderate inflammation-induced fetal programming during maternal stress conditions to consider the impact on fetal survival mechanisms in addition to potential benefits for postnatal health and growth performance.

LITERATURE CITED

Aaltonen, R., T. Heikkinen, K. Hakala, K. Laine, and A. Alanen. 2005. Transfer of proinflammatory cytokines across term placenta. Obstet. Gynecol. 106:802–807. doi:10.1097/01.AOG.0000178750.84837.ed

Ardestani, P. M., A. K. Evans, B. Yi, T. Nguyen, L. Coutellier, and M. Shamloo. 2017. Modulation of neuroinflammation and pathology in the 5XFAD mouse model of Alzheimer's disease using a biased and selective beta-1 adrenergic receptor partial agonist. Neuropharmacology 116:371–386. doi:10.1016/j.neuropharm.2017.01.010

Bloise, E., M. Bhuiyan, M. C. Audette, S. Petropoulos, M. Javam, W. Gibb, and S. G. Matthews. 2013. Prenatal endotoxemia and placental drug transport in the mouse: Placental size-specific effects. PLoS One 8:e65728. doi:10.1371/journal.pone.0065728

Bodie, K., W. R. Buck, J. Pieh, M. J. Liguori, and A. Popp. 2016. Biomarker evaluation of skeletal muscle toxicity following clofibrate administration in rats. Exp. Toxicol. Pathol. 68:289–299. doi:10.1016/j.etp.2016.03.001

Cadaret, C. N., K. A. Beede, H. E. Riley, and D. T. Yates. 2017. Acute exposure of primary rat soleus muscle to zilpaterol HCl (β2 adrenergic agonist), TNFα, or IL-6 in culture increases glucose oxidation rates independent of the impact on insulin signaling or glucose uptake. Cytokine 96:107–113. doi:10.1016/j.cyto.2017.03.014

Church, J. E., J. Trieu, R. Sheorey, A. Y. Chee, T. Naim, D. M. Baum, J. G. Ryall, P. Gregorevic, and G. S. Lynch. 2014. Functional β-adrenoceptors are important for early muscle regeneration in mice through effects on myoblast proliferation and differentiation. PLoS One 9:e101379. doi:10.1371/journal.pone.0101379

Cotechini, T., W. J. Hopman, and C. H. Graham. 2014a. Inflammation-induced fetal growth restriction in rats is associated with altered placental morphometrics. Placenta 35:575–581. doi:10.1016/j.placenta.2014.05.002

Cotechini, T., M. Komisarenko, A. Sperou, S. Macdonald-Goodfellow, M. A. Adams, and C. H. Graham. 2014b. Inflammation in rat pregnancy inhibits spiral artery remodeling leading to fetal growth restriction and features of preeclampsia. J. Exp. Med. 211:165–179. doi:10.1084/jem.20130295

Depner, T. A. 2001. Uremic toxicity: Urea and beyond. Seminars in dialysis. 14(4):246–251. doi:10.1046/j.1525-139X.2001.00072.x

Dogra, C., H. Changotra, S. Mohan, and A. Kumar. 2006. Tumor necrosis factor-like weak inducer of apoptosis inhibits skeletal myogenesis through sustained activation of nuclear factor-kappaB and degradation of MyoD protein. J. Biol. Chem. 281:10327–10336. doi:10.1074/jbc.M511131200

Du, H., C. H. Shih, M. N. Wosczyna, A. A. Mueller, J. Cho, A. Aggarwal, T. A. Rando, and B. J. Feldman. 2017. Macrophage-released ADAMTS1 promotes muscle stem cell activation. Nat. Commun. 8:669. doi:10.1038/s41467-017-00522-7

Frost, R. A., C. H. Lang, and M. C. Gelato. 1997. Transient exposure of human myoblasts to tumor necrosis factor-alpha inhibits serum and insulin-like growth factor-I stimulated protein synthesis. Endocrinology 138:4153–4159. doi:10.1210/endo.138.10.5450

He, X., Z. Xie, Q. Dong, J. Li, W. Li, and P. Chen. 2015. Effect of folic acid supplementation on renal phenotype and epigenotype in early weanling intrauterine growth retarded rats. Kidney Blood Press. Res. 40:395–402. doi:10.1159/000368516

Hoene, M., H. Runge, H. U. Häring, E. D. Schleicher, and C. Weigert. 2013. Interleukin-6 promotes myogenic differentiation of mouse skeletal muscle cells: Role of the STAT3 pathway. Am. J. Physiol. Cell Physiol. 304:C128–C136. doi:10.1152/ajpcell.00025.2012

Jensen, E. C., J. E. Harding, M. K. Bauer, and P. D. Gluckman. 1999. Metabolic effects of IGF-I in the growth retarded fetal sheep. J. Endocrinol. 161:485–494.

Kharraz, Y., J. Guerra, C. J. Mann, A. L. Serrano, and P. Muñoz-Cánoves. 2013. Macrophage plasticity and the role of inflammation in skeletal muscle repair. Mediators Inflamm. 2013:491497. doi:10.1155/2013/491497

Kitzmann, M., G. Carnac, M. Vandromme, M. Primig, N. J. Lamb, and A. Fernandez. 1998. The muscle regulatory factors MyoD and myf-5 undergo distinct cell cycle-specific expression in muscle cells. J. Cell Biol. 142:1447–1459. doi:10.1083/jcb.142.6.1447

Kohmura, Y., T. Kirikae, F. Kirikae, M. Nakano, and I. Sato. 2000. Lipopolysaccharide (LPS)-induced intra-uterine fetal death (IUFD) in mice is principally due to maternal cause but not fetal sensitivity to LPS. Microbiol. Immunol. 44:897–904. doi:10.1111/j.1348-0421.2000.tb02581.x

Kolmus, K., M. Van Troys, K. Van Wesemael, C. Ampe, G. Haegeman, J. Tavernier, and S. Gerlo. 2014. B-agonists selectively modulate proinflammatory gene expression in skeletal muscle cells via non-canonical nuclear crosstalk mechanisms. Plos One 9:e90649. doi:10.1371/journal.pone.0090649

Lam, S. Y., G. L. Tipoe, E. C. Liong, and M. L. Fung. 2008. Chronic hypoxia upregulates the expression and function of proinflammatory cytokines in the rat carotid body. Histochem. Cell Biol. 130:549–559. doi:10.1007/s00418-008-0437-4

Langen, R. C., A. M. Schols, M. C. Kelders, E. F. Wouters, and Y. M. Janssen-Heininger. 2001. Inflammatory cytokines inhibit myogenic differentiation through activation of nuclear factor-kappaB. Faseb J. 15:1169–1180. doi:10.1096/fj.00-0463

Langen, R. C., J. L. Van Der Velden, A. M. Schols, M. C. Kelders, E. F. Wouters, and Y. M. Janssen-Heininger. 2004. Tumor necrosis factor-alpha inhibits myogenic differentiation through MyoD protein destabilization. Faseb J. 18:227–237. doi:10.1096/fj.03-0251com

Lemons, J. A., and R. L. Schreiner. 1983. Amino acid metabolism in the ovine fetus. Am. J. Physiol. 244:E459–E466. doi:10.1152/ajpendo.1983.244.5.E459

Lirussi, F., Z. Rakotoniaina, S. Madani, F. Goirand, M. Breuiller-Fouché, M. J. Leroy, P. Sagot, J. J. Morrison, M. Dumas, and M. Bardou. 2008. ADRB3 adrenergic receptor is a key regulator of human myometrial apoptosis and inflammation during chorioamnionitis. Biol. Reprod. 78:497–505. doi:10.1095/biolreprod.107.064444

Liu, L., J. A. Fissel, A. Tasnim, J. Borzan, A. Gocke, P. A. Calabresi, and M. H. Farah. 2016. Increased TNFR1 expression and signaling in injured peripheral nerves of mice with reduced BACE1 activity. Neurobiol. Dis. 93:21–27. doi:10.1016/j.nbd.2016.04.002

Nie, J., T. K. Tong, K. George, F. H. Fu, H. Lin, and Q. Shi. 2011. Resting and post-exercise serum biomarkers of cardiac and skeletal muscle damage in adolescent runners. Scand. J. Med. Sci. Sports 21:625–629. doi:10.1111/j.1600-0838.2010.01096.x

Posont, R. J., K. A. Beede, S. W. Limesand, and D. T. Yates. 2018. Changes in myoblast responsiveness to TNFα and IL-6 contribute to decreased skeletal muscle mass in intrauterine growth restricted fetal sheep. Transl. Anim. Sci. 2 (Suppl 1):S44–S47. doi:10.1093/tas/txy038

Rawls, A., J. H. Morris, M. Rudnicki, T. Braun, H. H. Arnold, W. H. Klein, and E. N. Olson. 1995. Myogenin's functions do not overlap with those of MyoD or Myf-5 during mouse embryogenesis. Dev. Biol. 172:37–50. doi:10.1006/dbio.1995.0004

Rozance, P. J., L. Zastoupil, S. R. Wesolowski, D. A. Goldstrohm, B. Strahan, M. Cree-Green, M. Sheffield-Moore, G. Meschia, W. W. Hay, Jr, R. B. Wilkening, et al. 2018. Skeletal muscle protein accretion rates and hindlimb growth are reduced in late gestation intrauterine growth-restricted fetal sheep. J. Physiol. 596:67–82. doi:10.1113/JP275230

Rudnicki, M. A., P. N. Schnegelsberg, R. H. Stead, T. Braun, H. H. Arnold, and R. Jaenisch. 1993. MyoD or Myf-5 is required for the formation of skeletal muscle. Cell 75:1351–1359. doi:10.1016/0092-8674(93)90621-V

Seo, K. H., J. W. Choi, H. S. Jung, H. Yoo, and J. D. Joo. 2017. The effects of Remifentanil on expression of high mobility group box 1 in septic rats. J. Korean Med. Sci. 32:542–551. doi:10.3346/jkms.2017.32.3.542

Yates, D. T., C. N. Cadaret, K. A. Beede, H. E. Riley, A. R. Macko, M. J. Anderson, L. E. Camacho, and S. W. Limesand. 2016. Intrauterine growth-restricted sheep fetuses exhibit smaller hindlimb muscle fibers and lower proportions of insulin-sensitive type I fibers near term. Am. J. Physiol. Regul. Integr. Comp. Physiol. 310:R1020–R1029. doi:10.1152/ajpregu.00528.2015

Yates, D. T., D. S. Clarke, A. R. Macko, M. J. Anderson, L. A. Shelton, M. Nearing, R. E. Allen, R. P. Rhoads, and S. W. Limesand. 2014. Myoblasts from intrauterine growth-restricted sheep fetuses exhibit intrinsic deficiencies in proliferation that contribute to smaller semitendinosus myofibres. J. Physiol. 592:3113–3125. doi:10.1113/jphysiol.2014.272591

Yates, D. T., A. S. Green, and S. W. Limesand. 2011. Catecholamines mediate multiple fetal adaptations during placental insufficiency that contribute to intrauterine growth restriction: Lessons from hyperthermic sheep. J. Pregnancy 2011:740408. doi:10.1155/2011/740408

Yates, D. T., A. R. Macko, M. Nearing, X. Chen, R. P. Rhoads, and S. W. Limesand. 2012. Developmental programming in response to intrauterine growth restriction impairs myoblast function and skeletal muscle metabolism. J. Pregnancy 2012:631038. doi:10.1155/2012/631038

Yates, D. T., J. L. Petersen, T. B. Schmidt, C. N. Cadaret, T. L. Barnes, R. J. Posont, and K. A. Beede. 2018. ASAS-SSR triennnial reproduction symposium: Looking back and moving forward-how reproductive physiology has evolved: Fetal origins of impaired muscle growth and metabolic dysfunction: Lessons from the heat-stressed pregnant ewe. J. Anim. Sci. 96:2987–3002. doi:10.1093/jas/sky164

Zhu, M. J., S. P. Ford, P. W. Nathanielsz, and M. Du. 2004. Effect of maternal nutrient restriction in sheep on the development of fetal skeletal muscle. Biol. Reprod. 71:1968–1973. doi:10.1095/biolreprod.104.034561